J Comput Aided Mol Des (2011) 25:753–762
DOI 10.1007/s10822-011-9458-5

Active site similarity between human and *Plasmodium falciparum* phosphodiesterases: considerations for antimalarial drug design

Brittany L. Howard · Philip E. Thompson · David T. Manallack

Received: 31 March 2011 / Accepted: 8 July 2011 / Published online: 16 July 2011

Abstract The similarity between *Plasmodium falciparum* phosphodiesterase enzymes (*Pf*PDEs) and their human counterparts have been examined and human PDE9A was found to be a suitable template for the construction of homology models for each of the four *Pf*PDE isoforms. In contrast, the architecture of the active sites of each model was most similar to human PDE1. Molecular docking was able to model cyclic guanosine monophosphate (cGMP) substrate binding in each case but a docking mode supporting cyclic adenosine monophosphate (cAMP) binding could not be found. Anticipating the potential of *Pf*PDE inhibitors as anti-malarial drugs, a range of reported PDE inhibitors including zaprinast and sildenafil were docked into the model of *Pf*PDEα. The results were consistent with their reported biological activities, and the potential of PDE1/9 inhibitor analogues was also supported by docking.

Keywords Malaria · *Plasmodium falciparum* · Phosphodiesterase · Homology modelling · Molecular modelling · Molecular docking

Dedicated to the memory of Kate Burt.

Electronic supplementary material The online version of this article (doi:10.1007/s10822-011-9458-5) contains supplementary material, which is available to authorized users.

B. L. Howard · P. E. Thompson · D. T. Manallack (✉)
Medicinal Chemistry and Drug Action, Monash Institute of Pharmaceutical Sciences, Monash University, 381 Royal Parade, Parkville, VIC 3052, Australia
e-mail: David.Manallack@monash.edu

Introduction

Malaria is an infectious disease caused by protozoan parasites and is transmitted through the bite of infected female Anopheles mosquitoes [1, 2]. The malaria parasite belongs to the genus *Plasmodium*, with the majority of human infections caused by four species (*P. falciparum*, *P. vivax*, *P. malariae*, and *P. ovale*). *P. falciparum* is the most pathogenic form and the only species where life-threatening complications such as cerebral malaria, severe anaemia and renal failure are frequently seen [3]. The life-cycle of *P. falciparum* consists of complex sexual stages in the mosquito and asexual replicating stages in the human host [4].

Despite the range of drug therapies available (including quinolines, artemisinins, antifolates, atovaquone/proguanil combinations, and antibiotics), there is a paucity of simple and effective drug regimes for treating malaria. More importantly, drug resistance in *P. falciparum* has limited the number of viable treatment options [5, 6]. The challenge therefore faced by the drug discovery community is to find new targets in an effort to help treat malaria. Great advances have been made in genomics and the provision of laboratory methods to enable research into parasite life cycles. Recent work has looked at further interventions in the blood and liver stages as well as the potential for developing a range of vaccines [7].

While targeting essential metabolic pathways that are present in the parasite but absent or non-essential in the human host has had some success, the alternative approach is to seek targets common to both organisms for which a range of human therapeutic substances have been developed. An example of the latter strategy is to target phosphodiesterase (PDE) enzymes [8]. The PDEs are a superfamily of metal ion-dependent enzymes whose primary role is to terminate the cyclic nucleotide second

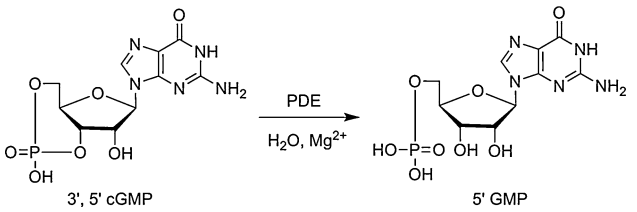

Fig. 1 Reaction catalysed by phosphodiesterase illustrated with cGMP as the substrate

messenger signal within a cell through hydrolysis of the 3′-phosphoester bond of cyclic adenosine monophosphate (cAMP) and cyclic guanosine monophosphate (cGMP; Fig. 1) [9–11].

Four PDEs (*Pf*PDEα-δ) are present in the genome of *P. falciparum* which have been cloned and characterised [12–14]. Furthermore, various studies have indicated that cyclic nucleotides are likely to play a major role in the cell biology of *P. falciparum* (including sexual development, hepatocyte infection, gametocytogenesis, cell cycle control, and exocytosis) [15, 16]. As a consequence, it has been suggested that targeting *P. falciparum* PDEs should disrupt a range of physiological processes and weaken or kill the organism [15–19]. Interest in this area has been focussed on understanding the role of PDEs in the parasite life cycle [15, 16, 20]. In addition, Yuasa and co-workers have screened compounds against *Pf*PDEα which has identified potential starting points for medicinal chemistry [21]. Interestingly, zaprinast was able to inhibit *Pf*PDEα with an IC_{50} of 3.8 μM and to inhibit parasite proliferation with an EC_{50} of 35 μM [21]. More recently, Beghyn and co-workers [22] developed a series of tadalafil analogues as potential inhibitors of *Pf*PDEs with the best compound (Fig. 2) showing potent antiplasmodial activity (IC_{50} 0.5 μM). Additional work on these compounds is required to determine whether blockade of *Pf*PDEs was responsible for the inhibition of proliferation. Certainly, the provision of more potent and selective compounds will aid this research.

As crystal structures of *P. falciparum* PDEs have yet to be described, homology models of these enzymes based on a human PDE template could facilitate our drug discovery efforts. The human genome encodes for 21 PDEs that are classified into 11 families, with up to 46% sequence homology at the amino acid level [14, 23–25]. This current study has focussed on the generation of *Pf*PDE homology models for each of the four isoforms. Molecular docking experiments have also been undertaken to gain insights into cyclic nucleotide selectivity and the binding modes of known inhibitors.

Computational methods

Sequence alignment, template selection

Protein sequences of both human and malarial PDEs were retrieved from the UniProtKB database [26]. The Lalign [27] global alignment method was employed to compare sequences to determine percentage homologies and to suggest likely alignments. Further adjustments to the sequence alignments were undertaken to coincide with previous work in our laboratories [28] (suppl. data). Usually this involved moving gaps out of helical regions to loop sections. This optimised alignment utilised the 16 amino acids known to be conserved among the human enzymes as a guide to give the appropriate overlay of these invariant residues. These adjustments align residues that play a key structural role in the protein. From these analyses potential template proteins were identified and additional criteria were examined to select the most appropriate crystal structure for homology modelling purposes.

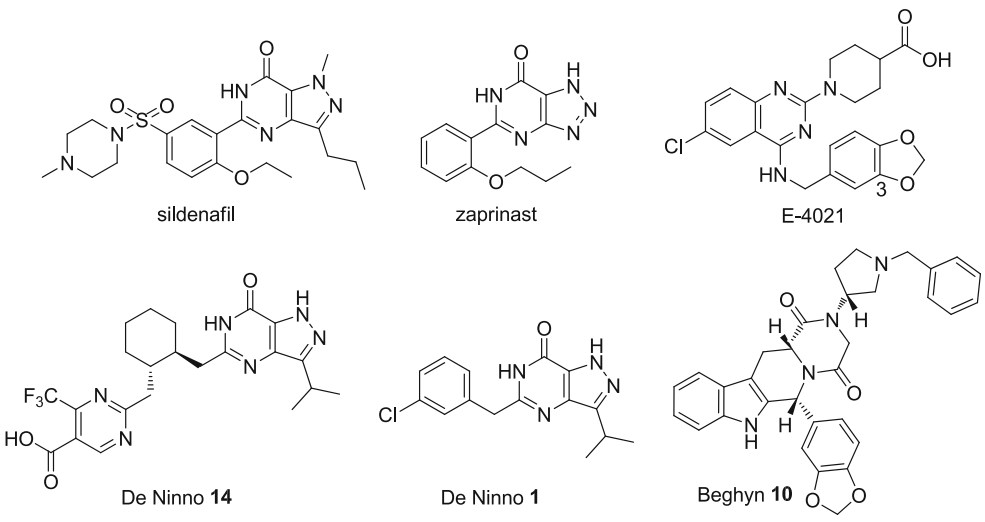

Fig. 2 Structures of the ligands used in the docking studies. Compounds De Ninno **1** and De Ninno **14** were taken from the study by De Ninno and co-workers [31] while compound Beghyn 10 was taken from the research recently described by Beghyn et al. [22], and in each case utilises their numbering schemes

Model building and minimisation

Each homology model was generated using Prime version 2.2 (Maestro version 9.1, Schrödinger, LLC, New York, USA) employing the optimised sequence alignment. The model building process used the PDE9A structure 3DYN [29] and retained the endogenous cGMP ligand, metal ions together with their coordinated water molecules. Minimisation of the model was undertaken using Macromodel version 9.8 (Maestro version 9.1, Schrödinger, LLC, New York, USA), employing the PRCG method and the OPLS_2005 force field. Initially, amino acid side chains were minimised with the ligand, metals, water molecules and protein backbone held rigid. Steric clashes were addressed by the rotation of strained residues. Typically this was a result of the substitution of a smaller amino acid for a larger one and manual inspection was required to look for alternative conformations to reduce steric strain. This involved examining other PDE crystal structures with similar amino acids in these positions to provide clues to likely low energy conformations. Following this, the model was further minimised while maintaining the previous constraints. A final minimisation was conducted without constraints and the models were assessed using MolProbity [30] which included a Ramachandran analysis.

Docking

Docking was performed using Glide version 5.6 (Maestro version 9.1, Schrödinger, LLC, New York, USA) employing the XP (extra precision) mode. Both cyclic nucleotides (cAMP and cGMP) were docked into each *Pf*PDE model. In each case, two conformations of the terminal carboxamide of the invariant purine-scanning glutamine (Gln453; the numbering used in this study refers to the 3DYN crystal structure [29]) were explored. Additionally, each cyclic nucleotide was minimized in the protein using both conformations of the carboxamide of the purine-scanning glutamine. This was undertaken to gain insight into the conformation of this residue and was applied to the docking of a series of PDE inhibitors (Fig. 2).

Results and discussion

The similarity between *h*PDE and *Pf*PDE has been previously recognized and Wentzinger and Seebeck suggested that the sequences of the *Pf*PDEs conformed to the general Class I grouping of the mammalian PDEs [32]. This is indirectly supported by the crystal structure of *Leishmania major* (*Lmj*PDEB1) which similarly adopts the general fold of the Class I PDEs, drawing the link between mammalian and protozoan PDEs [33].

The full-length PDE proteins have been depicted as having three regions: an N-terminal splicing region, a regulatory domain, and a C-terminal catalytic domain. Within the catalyic domain of each PDE enzyme are 16 α-helices which can be further divided into three subdomains (helices 1–7, 8–11, and 12–16). The active site exists at the interface of the three subdomains, where 11 of the 16 invariant amino acids of the catalytic domain are situated [34]. The catalytic site consists of four subsites that influence substrate binding: a metal-binding site (M-site), core pocket (Q pocket), hydrophobic pocket (H pocket) and lid region (L region) [24].

Protein sequence comparison

An examination of the full length *Pf*PDE sequences has predicted that they contain three to six transmembrane helices, suggesting that they are integral membrane proteins [28]. Sequence analysis of these full length *Pf*PDEs has also shown that they represent a new PDE family [21]. Interestingly, they show a low degree of relatedness to *h*PDE9A as well as *Dictyostelium* PDE, RegA [21] from an evolutionary perspective. An analysis of the catalytic domains of the four *Pf*PDEs showed that their sequence identities varied from 25 to 37% (Table 1). Again the *Pf*PDEs did not fall into any known human PDE families when these catalytic domains were compared in isolation. On average, the four *Pf*PDEs showed a sequence identity of 23% to the human PDEs, with approximately 50% of residues being indicated as highly similar. *Lmj*PDEB1 showed 26% average sequence identity with the human PDEs which was in contrast to its similarity to the *Pf*PDEs (22%). Given that the sequence identities were quite low and did not vary considerably across the human PDEs, the choice of template for the *Pf*PDEs was influenced by the earlier finding of the evolutionary relatedness between the *Pf*PDEs and *h*PDE9A. The comparison of *h*PDE9A to *Pf*PDEα showed a 27% sequence identity with just over 50% of residues being considered highly similar.

There are 16 amino acids that are absolutely conserved among the 21 human PDE enzymes, and of these 13 are also fully conserved across the series of four *Pf*PDE enzymes. The changes that would result from the lack of conservation of the three outstanding residues are not expected to alter the gross structure of the proteins. An invariant asparagine in human enzymes (N253) at the beginning of helix 6 is conserved in *Pf*PDEβ, γ and δ but was found to be a threonine residue in *Pf*PDEα. In the *h*PDEs this asparagine residue may provide structural stability to the enzyme by forming a hydrogen bond with adjacent backbone amides of isoleucine, valine and alanine residues. Within helix 9, serine replaces a conserved alanine (A312) in *Pf*PDEα, β and γ. This alanine residue is

Table 1 Percent homologies of human and protozoan PDE enzymes

		*Pf*PDEα	*Pf*PDEβ	*Pf*PDEγ	*Pf*PDEδ	*Lmj*PDEB1
*Pf*PDE	α					21.9
	β	30.9				23.1
	γ	29.8	36.8			21.9
	δ	25.3	27.8	27		21.1
*h*PDE	1A	21.2	26.7	24.6	21.1	24
	1B	23.6	25.8	26.3	21.9	24.6
	1C	20.9	25.2	25.8	22.7	24.1
	2A	23.9	24.9	24.3	18.4	28.3
	3A	22.6	22.8	23.9	20.2	21.4
	3B	21.2	23.1	24.9	20	23.2
	4A	24.1	24.9	25.6	19.9	27.7
	4B	25.4	24.4	26.5	18.9	28
	4C	23.9	24.7	26.8	20.6	27.9
	4D	24.3	25.6	27.4	18.2	27.6
	5A	19.9	23.3	22.5	20.2	27.8
	6A	20.4	21.8	22.4	17.4	25.7
	6B	21.5	23.2	23	16.5	24.9
	6C	20.3	23.8	23	18.5	26
	7A	26.5	27.3	24.6	22.5	26.9
	7B	21.6	24.8	22.1	23.2	26
	8A	22.5	24	26.4	21.3	26.2
	8B	23.2	24	26.1	19.2	26.4
	9A	26.8	27.5	23.1	21.1	25.7
	10A	20.9	22.9	22.1	17.6	26.4
	11A	21.3	25.8	23.4	18.2	30.7

positioned in a cavity on the outside of the protein where there is sufficient room to accommodate the additional hydroxyl group of the serine. Thirdly, histidine (H324) in helix 10 is replaced by a tyrosine residue in all four *Pf*PDEs and appears to be coupled to a complementary change at an acidic residue (usually aspartic acid; PDE1 is the only exception, where it is a glutamic acid) between helices 7 and 8 (D295). This acidic residue in human enzymes is replaced with a glycine residue in the *Pf*PDE enzymes that presumably allows room for the larger tyrosine residue.

Homology models

Homology models of the four *Pf*PDEs were constructed based on the co-ordinates of the *h*PDE9A crystal structure (pdb code: 3DYN) [29]. In this structure, *h*PDE9A is in complex with the endogenous ligand cGMP at 2.10 Å resolution [29]. When superimposed onto the *h*PDE9A crystal structure template (Fig. 3), the only noticeable deviations from that structure arose from small insertions in the loop regions. These insertions were not in close proximity to the binding site in any of the models generated and would not be expected to significantly affect substrate or inhibitor binding. Each of the models was assessed using MolProbity [30] and a Ramachandran plot analysis (suppl. data) that showed backbone phi and psi angles in the expected regions and required no further refinement.

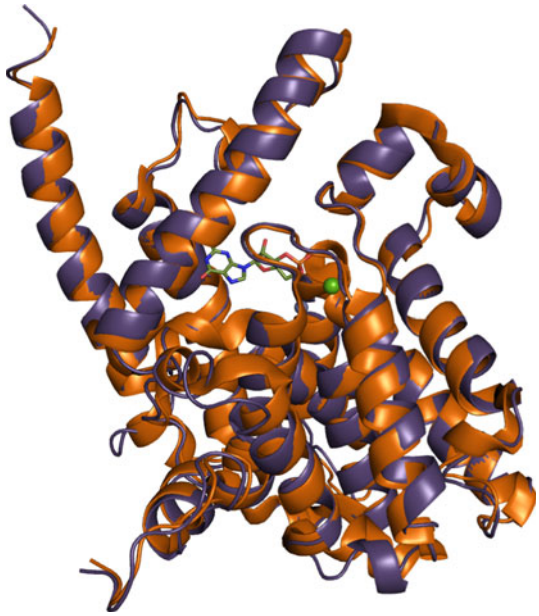

Fig. 3 Overlay of the fully minimised *Pf*PDEα homology model (*light*) with the 3DYN crystal structure (*dark*) [29]

*h*PDE binding sites are characterised primarily by a critical conserved purine-scanning glutamine (Gln453) residue and 'hydrophobic clamp' comprised of an aromatic purine-stacking residue at the roof of the binding site (Phe456) and a hydrophobic residue, isoleucine, valine or leucine at the bottom of the site (Leu420, R5 in Table 2) [11, 23, 25, 28]. This forms the basis of adenine or guanine binding of the cyclic nucleotides.

The models in this study were built retaining cGMP, the metal ions and coordinated water molecules in the binding site to ensure that the binding cavity would not collapse during the building or minimisation of the models. This helped maintain the integrity of the hydrogen bond network within the site, and ensured the hydrophobic clamp remained in position. Thus the resultant models are constructed around these features, yielding a cGMP substrate bound conformer of the *Pf*PDEs. Removal of the endogenous ligand and subsequent full minimisation did not result in any significant change to the positions of the metal ions nor to the shape or volume of the binding cavity (Fig. 4; suppl. data). These 'cGMP-specific' models were considered to be suitable for further modelling work, as experimental work by Yuasa and co-workers had previously shown *Pf*PDEα to be cGMP specific [21].

Table 2 A list of the 25 residues associated with the active site of human, *P. falciparum* and *L. major* PDEs

3DYN residue number		Region	Phosphodiesterase															
			Human											*P. falciparum*				*L. major*
			1 (A, B, C)	2	3	4	5	6	7 (A, B)	8	9	10	11	α	β	γ	δ	B1
292	(i)	M	H	H	H	H	H	H	H	H	H	H	H	H	H	H	H	H
293	(i)	M	D	D	D	D	D	D	D	D	D	D	D	D	D	D	D	D
296	(i)	M	H	H	H	H	H	H	H	H	H	H	H	H	H	H	H	H
322	(i)	M	E	E	E	E	E	E	E	E	E	E	E	E	E	E	E	E
325	(i)	M	H	H	H	H	H	H	H	H	H	H	H	H	H	H	H	H
402	(i)	M	D	D	D	D	D	D	D	D	D	D	D	D	D	D	D	D
251	(R3)	Q	Y	Y	Y	Y	Y	Y	Y	Y	F	Y	Y	Y	Y	Y	Y	Y
405	(R1)	Q	H	D	G	N	A	A	N	N	N	S	A	H	H	H	H	N
413	(R2)	Q	H	T	H	Y	Q	Q	S	C	A	T	S	H	H	H	H	S
420	(R5)	Q + H	L	I	I	I	V	V	V	I	L	I	V	I	V	L	V	V
423	(i)	Q	E	E	E	E	E	E	E	E	E	E	E	E	E	E	E	E
453	(R6) (i)	Q	Q	Q	Q	Q	Q	Q	Q	Q	Q	Q	Q	Q	Q	Q	Q	Q
456		Q	F	F	F	F	F	F	F	F	F	F	W	F	F	F	F	F
490	(R7)	Q	W	W	W	Y	W	W	W	W	Y	W	W	W	W	W	W	I
421		H	M, L, M	Y	V	M	A	A	T, C	S	L	Y	T	N[a]	L	V	S	T
424		H	F	F	F	F	F	F	F	Y	Y	F	F	F	F	F	F	F
441		H	L (ii)	M	F	M	L	M	L	V	F	M	I	C[a]	L	L	I	M
301		L	N	N	N	N	N	N	Q	N	N	N	N	N	N	N	N	N
302		L	N, N, S	S	A	Q	S	L	P	S	T	S	A	Y[a]	L	I	S	S
303		L	F	F	F	F	Y	Y	F	F	Y	Y	Y	F	F	F	Y	F
452		L	S	L	L	S	M	L	I	S	A	G	L	S	S	I[c]	T[d]	G
455		L	G	S	S	G	G	G	G	S	G	G	E	D[a]	T	T	Y[d]	G
459		L	F	H	H	Y	A	F	Y	Y	F	A	S	H	F	E[c]	I[d]	F
406	(R8)	(iii)	P	Q	P	P	I	I	P	P	E	V	V	S[a]	G[b]	N[c]	T[d]	V
417	(R4)	(iii)	T	A	T	T	A	A	S	A	V	A	A	T	C[b]	V	T	A

Numbering is based on the 3DYN pdb crystal structure [29]. (i) indicates an invariant residue, (ii) while a list of amino acids has been compiled for this hydrophobic region position, this amino acid falls in a loop region. Each of the PDEs have differing lengths for this loop and thus in a 3-dimensional sense it may be difficult to make comparisons. Having said that, PDEs 3, 4, 5 and 9 overlay quite well while PDE1 is distorted at this point, (iii) no region assigned to this residue. R numbers in brackets refers to numbering from ref [28]

[a] Residue as unique to *Pf*PDEα at this position

[b] Residue as unique to *Pf*PDEβ at this position

[c] Residue as unique to *Pf*PDEγ at this position

[d] Residue as unique to *Pf*PDEδ at this position

Active site analysis

With models established that preserved the basic fold of the PDE catalytic domain, we then examined the residues associated with the active site of the *Pf*PDEs. This may be a means to predict or understand the cyclic nucleotide or inhibitor selectivity of the isozymes. Firstly, the sequence similarity of the cyclic nucleotide binding site was assessed by sequence alignment on the key residues in the M (metal-binding), H (hydrophobic pocket), L (lid region) and Q (core pocket) regions (Table 2) as defined by Sung et al. [24]. Within the active site itself, the purine-stacking phenylalanine is conserved while at the opposite side of this site the amino acid (R5) varies between the following hydrophobic residues: isoleucine (α), valine (β, δ) and leucine (γ).

With regard to the purine-scanning glutamine residue (R6, Table 2), it has been shown that in human PDEs the terminal carboxamide group of this residue exists in either one of two conformations (through a 180° rotation) and forms complementary hydrogen bonds to either of the cyclic nucleotide substrates [25]. This 'glutamine switch' mechanism has been proposed to explain PDE substrate preference for cAMP and cGMP. Both cAMP- and cGMP-specific enzymes hold the glutamine in the appropriate conformation through a network of hydrogen bonds.

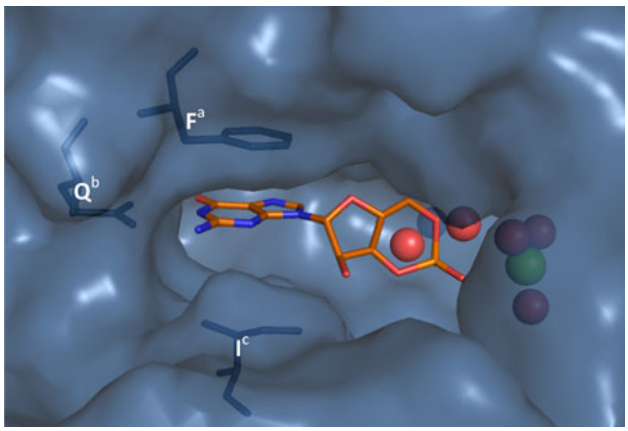

Fig. 4 Surface representation of the *Pf*PDEα binding site shown complexed with cGMP. Mg^{2+}, Zn^{2+} and water molecules are represented by spheres. The purine-scanning glutamine is also shown together with the hydrophobic clamp residues. [a]Equates to F456, [b]equates to Q453 and [c]equates to L420 using 3DYN numbering

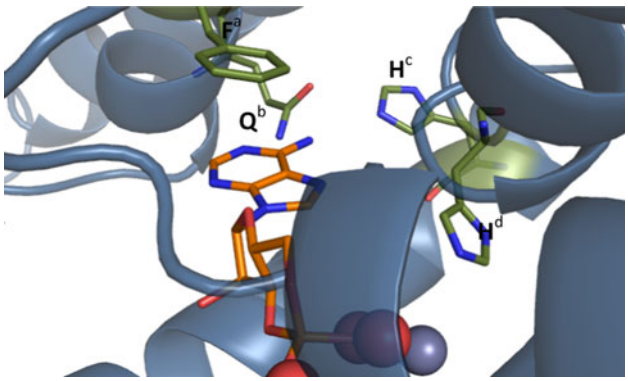

Fig. 5 Diagram illustrating the close arrangement of the purine-scanning glutamine (Q^b) and histidine (H^c) in the *Pf*PDEα active site. [a]Equates to F456, [b]equates to Q453, [c]equates to N405, and [d]equates to H413 using 3DYN numbering

PDE9A is a cGMP specific isozyme and the crystal structure shows that the purine-scanning glutamine residue (Gln453) is anchored via hydrogen-bonding to an adjacent glutamine (Gln406) which locks it into a cGMP-specific conformation. In dual-specific PDEs, the glutamine residue is free to rotate and adopt either conformation, allowing both cAMP and cGMP to bind as substrates [25].

The ability of the *Pf*PDEα models to accommodate cAMP was investigated through a manual rotation of the carboxamide group of the purine-scanning glutamine residue (R6, Table 2) and energy minimisation of the structure. Notably, a clash with the adjacent histidine residue (R2, Table 2) prevented the glutamine from presenting a conformer suitable for cAMP binding for any of the four *Pf*PDEs (Fig. 5). This clash could not be relieved by energy minimisation nor by any manual rotation of the histidine residues to accommodate cAMP. This may support the observation that *Pf*PDEα is cGMP specific [32]. As each *Pf*PDE shares histidine residues in positions R1 and R2, this suggests that they too may be cGMP selective. That none of the four identified isozymes can hydrolyse cAMP would be surprising given the apparent role of *Pf*PKA in parasite signalling [35].

Another region of interest is located next to the purine-scanning glutamine in the active site. In *Leishmania major* and *Trypanosoma* protozoa the residue preceding this glutamine is a glycine residue. This effectively opens up a pocket near the glutamine residue that is apparent only in *h*PDE10 and has been suggested as a selectivity pocket for drug design against these parasites [33]. As the *Pf*PDE enzymes do not share the glycine residue adjacent to the purine-scanning glutamine, it is presumed that the additional pocket found in *h*PDE10 and other protozoan enzymes will not exist in *Pf*PDEs.

This analysis has highlighted potentially important differences between *Pf*PDEs and *h*PDE9A from which the models were built. Most strikingly, the relationship to *h*PDE9A in the binding site is lost at positions R1 and R2 (Table 2) and all the *Pf*PDEs have two histidine residues that are only found in *h*PDE1. The relationship to *h*PDE1 is strongest for *Pf*PDEβ and *Pf*PDEγ (Table 2), and these latter two enzymes are highly similar (37%) to each other. *Pf*PDEα was found to be most similar to *h*PDE3 in this region, showing the same residues in positions R4 and R5 in the active site. *Pf*PDEα, β and γ also show binding site similarities to *h*PDE1 and *h*PDE3. *Pf*PDEδ in contrast, shows similarity to *h*PDEs 5, 6 and 11 and this may be attributed to residues within the lid region as well as position R5 (Val) in the active site. On balance however, the residues closely associated with the active site (i.e. R1–R8) suggest that the *Pf*PDEs appear to be mostly *h*PDE1-like (particularly residues R1 and R2).

Docking

The value of homology models is primarily to expedite the design of new inhibitors of *Pf*PDEs which will be the crucial tools for delineating isozyme function and validating the clinical potential of *Pf*PDE inhibition. To date the only pharmacological data relating to *Pf*PDE activity concerns a selection of PDE inhibitors screened against *Pf*PDEα [32]. Our plan is to perform large scale virtual screens of chemical libraries to enrich the selection of inhibitors prior to the availability of in vitro assays.

Seebeck and co-workers [32] reported the inhibitory activity of several PDE inhibitors against *Pf*PDEα. Of the compounds tested, the *h*PDE1/5 inhibitor, zaprinast (*h*PDE1 IC_{50} = 6 μM, *h*PDE5A IC_{50} = 0.81 μM, *h*PDE9A IC_{50} = 29–46 μM [36]) was the most potent inhibitor with an IC_{50} value of 3.8 μM [32]. The PDE inhibitors E4021 (*h*PDE5A

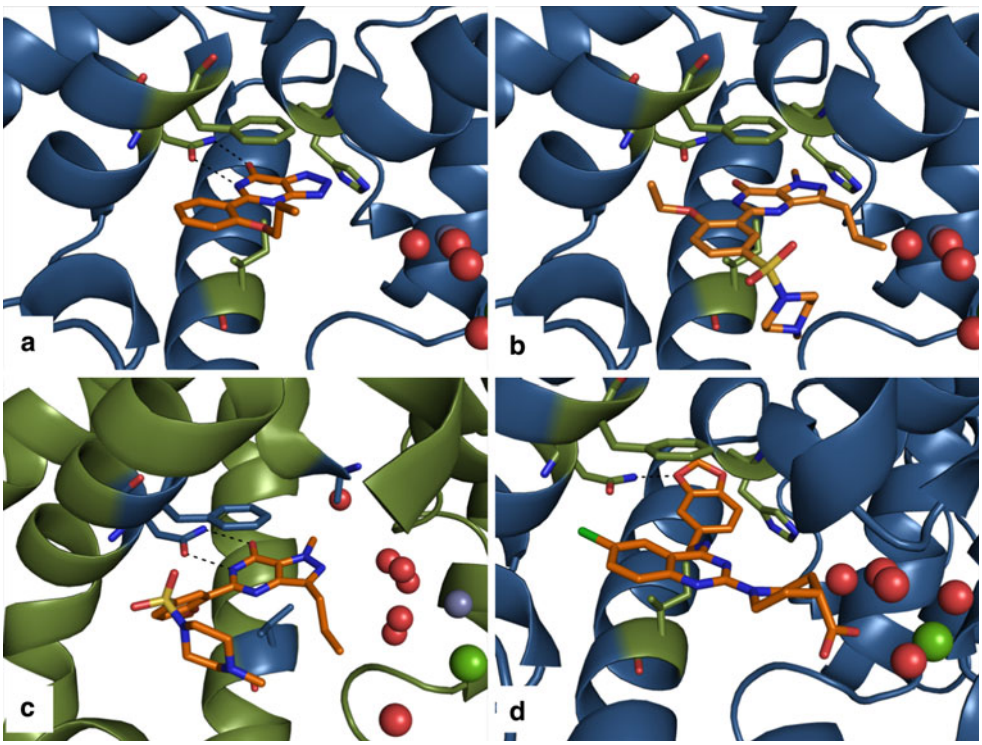

Fig. 6 **a** Zaprinast docked into the *Pf*PDEα model, **b** Sildenafil docked into the *Pf*PDEα model, **c** Sildenafil bound to the *h*PDE5A 1TBF crystal structure, and **d** E4021 docked into the *Pf*PDEα model. Purine-scanning glutamine, hydrophobic clamp and histidine residues are *highlighted*. Mg^{2+}, Zn^{2+} and water molecules are represented by *spheres*. Hydrogen bonds are shown with *dashed lines*

IC_{50} = 6.2 nM [36]) and sildenafil (*h*PDE5A IC_{50} = 1.6 nM, *h*PDE9A IC_{50} = 2.6–11 μM [36]) were also reported to exhibit moderate activity against *Pf*PDEα (IC_{50} values of 46 and 56 μM, respectively) [32].

When zaprinast was docked into the *Pf*PDEα models, it adopted a pose analogous to the binding of the pyrazolo-pyrimidinone core of sildenafil in the *h*PDE5A crystal structures, 1TBF [25] and 1UDT [24] (Fig. 6a). The expected contacts to the purine-scanning glutamine residue were evident, as well as aromatic stacking with the hydrophobic clamp. Furthermore, the pendant aryl groups superimpose, although the alkoxy groups project in different directions. The docked binding mode of sildenafil in the *Pf*PDEα model (Fig. 6b), while also similar to the *h*PDE5A crystal structure binding modes (1TBF [25] and 1UDT [24]; Fig. 6c), does not hydrogen bond as closely to the purine—scanning glutamine. This appears to be due to a clash between the histidine residue (R1, Table 2) and the pyrazole *N*-methyl substituent of sildenafil. In *h*PDE5A, the presence of a smaller alanine residue in this position avoids this clash. Interestingly, the bicyclic ring system of zaprinast lacks the *N*-methyl substituent and is thus able to fully enter the binding site to make the key interactions with the purine-scanning glutamine residue. Sildenafil also has additional interactions with the *h*PDE5A binding site through the bulky sulfonamide group that are not reproduced in *Pf*PDEα. Thus the docking mode of zaprinast appears convincing in light of crystal structures of sildenafil in *h*PDE5A and may explain the relative potency of the two molecules against *Pf*PDEα.

Very recently, Beghyn et al. [22] implemented a 'drug to genome to drug' approach to design and test a series of *Pf*PDE inhibitors based on tadalafil. Docking of compound 10 from the Beghyn study [22] (Fig. 2) was undertaken using our *Pf*PDEα model. Given that the binding mode of tadalafil in *h*PDE5A (pdb code 1XOZ) places the benzodioxole in a pocket adjacent to the purine-scanning glutamine residue [37], then a similar sized pocket would be required to successfully dock this compound into the *Pf*PDEα model. However, as the *Pf*PDE homology models do not possess a cavity of the right dimensions, the tadalafil analogues could not be successfully docked. Interestingly, the bottom of the *h*PDE5A benzodioxole binding pocket is lined with an alanine residue [A783, 1XOZ], while the *Pf*PDEs have larger amino acids in this position (N, L, V, S for α, β, γ and δ, respectively). In addition, the *h*PDE5A pocket in structure 1XOZ is made larger by the movement of helix 15 in a direction away from the metal atoms. The size of the amino acids, plus large scale protein movement results in a pocket that is capable of binding the benzodioxole group but this is precluded in our models. Clearly this requires further work to examine the amino acids lining this pocket as well as undertaking molecular dynamics experiments. This is the current subject of our research.

While crystal structures are not available to show the binding mode of E4021 in any available PDE enzyme, we

docked this ligand into the binding site of *Pf*PDEα. Docking suggests a binding mode for E4021 where the catechol ring system interacts with the purine-scanning glutamine through a single hydrogen bond and the piperidine carboxylic acid terminus resides near the metal ions of the binding site (Fig. 6d). In contrast, when E4021 was docked into the *h*PDE5A crystal structures 1UDT [24] and 1TBF [25], the binding mode showed that the ether oxygen in the 3-position formed a hydrogen bond with the purine-scanning glutamine.

Finally, as the sequence analyses comparing the human and *Pf*PDE enzymes showed similarity to both *h*PDE9A and *h*PDE1 (active site), we investigated a series of *h*PDE1/9 inhibitors recently reported by De Ninno and co-workers [31]. For example, compounds De Ninno **1** and **14** (Fig. 2) from that study were shown to have good activity at *h*PDE1 and 9, with compound **14** exhibiting useful selectivity for *h*PDE9A over *h*PDE1. When docked into each of the *Pf*PDE models, these compounds made two contacts to the purine-scanning glutamine residue and aromatic stacking with the purine-stacking phenylalanine in a manner similar to most PDE inhibitors. Like zaprinast, the pyrazolopyrimidinone core of De Ninno **1** and **14** was able to dock into the active site to form key interactions with the purine-scanning glutamine (Fig. 7). The same molecules could also be successfully docked into *h*PDE1 and *h*PDE9A structures, again making contacts to the purine-scanning glutamine and aromatic interactions with the purine-stacking phenylalanine.

Gaining selectivity for malarial PDEs

Prior studies on the *Pf*PDE biochemistry of zaprinast [32] and tadalafil analogues [22], as well as the docking of the *h*PDE9A and *h*PDE1 selective inhibitors described above show the potential for developing *Pf*PDE inhibitors from *h*PDE ligands. An important further element is the need to remove *h*PDE potency while retaining *Pf*PDE potency to achieve selectivity for the malarial PDEs. From the docking results it would appear that there may be several chemical fragments that could be explored to develop *Pf*PDE inhibitors such as the benzodioxole group of E4021 or the guanine mimics within zaprinast and sildenafil. It is clear however, that to obtain *Pf*PDE selectivity, binding site residues that are unique to the enzyme of interest need to be targeted. This approach has been successful in the development of highly selective and potent human PDE inhibitors [38]. It is therefore logical to target differences within the 25 binding residues associated with the active site (Table 2). Of the 25 amino acids, five residues within *Pf*PDEα are unique to this enzyme (Table 2, Fig. 8). We propose that targeting these particular residues will introduce selectivity for *Pf*PDEα over both human and other malarial PDEs. In a similar manner, targeting residues identified as being unique to *Pf*PDEβ, γ and δ (Table 2) may offer a means by which selectivity toward each isozyme may be achieved. Beghyn and co-workers [22] designed a set of tadalafil analogues where the N-methyl group was replaced with benzyl substituted pyrrolidine or

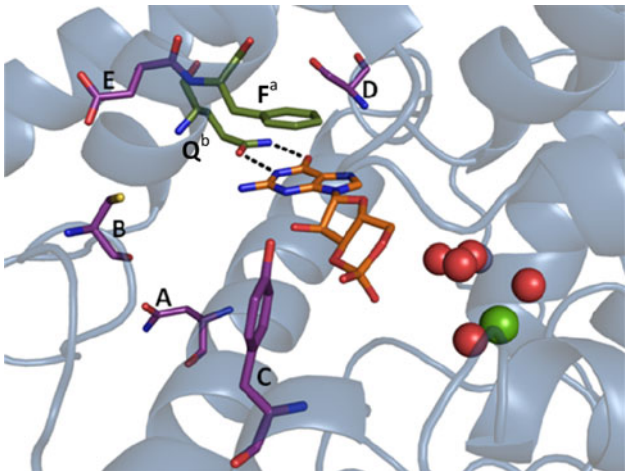

Fig. 8 Residues *A–E* (*highlighted*) that are unique to *Pf*PDEα that may offer a route to selectivity over other PDE enzymes if targeted through inhibitor design. [a]Equates to F456 and [b]equates to Q453 using 3DYN numbering. cGMP is shown within the active site. Mg^{2+}, Zn^{2+} and water molecules are represented by *spheres*. Hydrogen bonds are shown with *dashed lines*

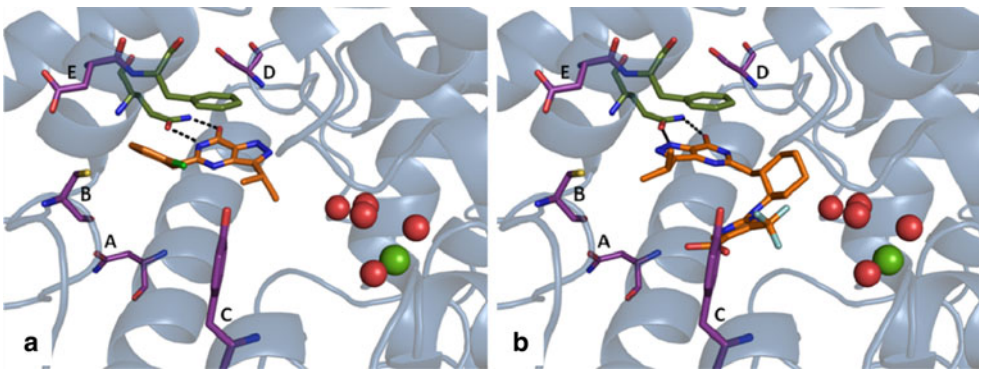

Fig. 7 **a** Docking of De Ninno **1** into the *Pf*PDEα model and **b** docking of De Ninno **14** into the *Pf*PDEα model. Mg^{2+}, Zn^{2+} and water molecules are represented by *spheres*. Hydrogen bonds are shown with *dashed lines*. Purine-scanning glutamine and purine-stacking phenylalanine residues are *highlighted*, as well as residues unique to *Pf*PDEα (*A–E*)

piperidine rings. These substituents are thought to be oriented towards the periphery of the active site where they can encounter residues unique to *Pf*PDEs. While further assays are needed to confirm their ability to inhibit *Pf*PDEs, these promising results are very positive and have encouraged us to continue our design and synthesis work.

Other means of introducing groups to gain selectivity may be gained by substitution from the 5-position of the guanine ring of cGMP and its related analogues to specifically target the R8 residue in the *Pf*PDEs (Residue E in Fig. 8). As the R8 residue is unique to each *Pf*PDE (Table 2), this simplistic approach could provide the basis for which selectivity may be obtained. Notwithstanding that their inhibitory potency is unknown, the De Ninno compounds **1** and **14**, which have been extended from this 2-position, show promising results when docked into each of the *Pf*PDE models (Fig. 7). The chlorobenzyl group at the 2-position of De Ninno **1** appears to extend toward the unique serine residue in *Pf*PDEα (residue D in Fig. 7). In the case of De Ninno **14**, docking favours an interaction between the pyrimidinetrifluoro carboxylic acid moiety and the metal binding site within the enzyme. Extending the molecule toward the unique tyrosine residue in each of the *Pf*PDEs (residue C in Fig. 7) should not be overlooked in the design strategy.

Conclusions

In anticipation of the potential of the four *Pf*PDE isozymes as targets for antimalarial drug design, we have constructed homology models based on gene sequence data and homology to their human counterparts. Interestingly, our models show that the binding site topology of the *Pf*PDEs have a high resemblance to *h*PDE1 and our modelling explains the cGMP selectivity of *Pf*PDEα. Docking of the reported *Pf*PDEα inhibitors zaprinast, E4021 and sildenafil, suggested plausible binding modes consistent with their relative potencies. Our docking studies also support the pursuit of *h*PDE1/9 inhibitors as starting points for the design of *Pf*PDEα inhibitors.

We hope that this information may provide a useful tool for screening compound libraries, either diversity-based or developed from the large PDE inhibitor pool. The generalized homology to *h*PDEs, coupled to observable differences in the binding sites might support structure-based design of pan-*Pf*PDE inhibitors that select against human isoforms, or also potentially *Pf*PDE-isoform selective inhibitors. The renewed fight against malaria requires the identification and validation of targets for therapy. With a pathway for conducting virtual screening for *Pf*PDEs, we hope that the road to finding molecules active against the parasite might be smoothed.

Acknowledgments The authors would like to thank Dr Paul Gilson for his helpful discussions.

References

1. Miller LH, Baruch DI, Marsh K, Doumbo OK (2002) Nature 415:673–679
2. Greenwood BM, Bojang K, Whitty CJ, Targett GA (2005) Lancet 365:1487–1498
3. Heddini A (2002) Int J Parasitol 32:1587–1598
4. Chiang PK, Bujnicki JM, Su X, Lanar DE (2006) Curr Mol Med 6:309–326
5. Woster PM (2003) New therapies for malaria. In: Doherty AM (ed) Annual reports in medicinal chemistry, vol 38. Elsevier, Amsterdam, pp 203–212
6. Ridley RG (2002) Nature 415:686–693
7. Kappe SH, Vaughan AM, Boddey JA, Cowman AF (2010) Science 328:862–866
8. Wentzinger L, Bopp S, Tenor H, Klar J, Brun R, Beck HP, Seebeck T (2008) Int J Parasitol 38:1625–1637
9. Lugnier C (2006) Pharmacol Ther 109:366–398
10. Conti M, Beavo J (2007) Ann Rev Biochem 76:481–511
11. Jeon YH, Heo YS, Kim CM, Hyun YL, Lee TG, Ro S, Cho JM (2005) Cell Mol Life Sci 62:1198–1220
12. Baker DA, Kelly JM (2004) Trends Parasitol 20:227–232
13. Gardner MJ, Hall N, Fung E, White O, Berriman M, Hyman RW, Carlton JM, Pain A, Nelson KE, Bowman S, Paulsen IT, James K, Eisen JA, Rutherford K, Salzberg SL, Craig A, Kyes S, Chan MS, Nene V, Shallom SJ, Suh B, Peterson J, Angiuoli S, Pertea M, Allen J, Selengut J, Haft D, Mather MW, Vaidya AB, Martin DM, Fairlamb AH, Fraunholz MJ, Roos DS, Ralph SA, McFadden GI, Cummings LM, Subramanian GM, Mungall C, Venter JC, Carucci DJ, Hoffman SL, Newbold C, Davis RW, Fraser CM, Barrell B (2002) Nature 419:498–511
14. Beavo JA (1995) Physiol Rev 75:725–748
15. Taylor CJ, McRobert L, Baker DA (2008) Mol Microbiol 69: 110–118
16. Moon RW, Taylor CJ, Bex C, Schepers R, Goulding D, Janse CJ, Waters AP, Baker DA, Billker O (2009) PLoS Pathog 5(9): e1000599
17. McRobert L, Taylor CJ, Deng W, Fivelman QL, Cummings RM, Polley SD, Billker O, Baker DA (2008) PLoS Biol 6(6):e139
18. Taylor HM, McRobert L, Grainger M, Sicard A, Dluzewski AR, Hopp CS, Holder AA, Baker DA (2010) Eukaryot Cell 9:37–45
19. Beraldo FH, Almeida FM, da Silva AM, Garcia CR (2005) J Cell Biol 170:551–557
20. Young JA, Fivelman QL, Blair PL, de la Vega P, Le Roch KG, Zhou Y, Carucci DJ, Baker DA, Winzeler EA (2005) Mol Biochem Parasitol 143:67–79
21. Yuasa K, Mi-Ichi F, Kobayashi T, Yamanouchi M, Kotera J, Kita K, Omori K (2005) Biochem J 392:221–229
22. Beghyn TB, Charton J, Leroux F, Laconde G, Bourin A, Cos P, Maes L, Deprez B (2011) J Med Chem 54:3222–3240
23. Ke H, Wang H (2007) Curr Top Med Chem 7:391–403
24. Sung BJ, Hwang KY, Jeon YH, Lee JI, Heo YS, Kim JH, Moon J, Yoon JM, Hyun YL, Kim E, Eum SJ, Park SY, Lee JO, Lee TG, Ro S, Cho JM (2003) Nature 425:98–102
25. Zhang KY, Card GL, Suzuki Y, Artis DR, Fong D, Gillette S, Hsieh D, Neiman J, West BL, Zhang C, Milburn MV, Kim SH, Schlessinger J, Bollag G (2004) Mol Cell 15:279–286
26. Fry M, Beesley J (1991) Parasitol Today 102:17–26
27. Chenna R, Sugawara H, Koike T, Lopez R, Gibson TJ, Higgins DG, Thompson JD (2003) Nucleic Acids Res 31:3497–3500

28. Manallack DT, Hughes RA, Thompson PE (2005) J Med Chem 48:3449–3462
29. Liu S, Mansour MN, Dillman KS, Perez JR, Danley DE, Aeed PA, Simons SP, Lemotte PK, Menniti FS (2008) Proc Natl Acad Sci USA 105:13309–13314
30. Chen VB, Arendall WB 3rd, Headd JJ, Keedy DA, Immormino RM, Kapral GJ, Murray LW, Richardson JS, Richardson DC (2010) Acta Crystallogr D Biol Crystallogr 66(Pt 1):12–21
31. De Ninno MP, Andrews M, Bell AS, Chen Y, Eller-Zarbo C, Eshelby N, Etienne JB, Moore DE, Palmer MJ, Visser MS, Yu LJ, Zavadoski WJ, Gibbs ME (2009) Bioorg Med Chem Lett 19:2537–2541
32. Wentzinger L, Seebeck T (2006) Protozoal phosphodiesterases. In: Beavo J (ed) Cyclic nucleotide phosphodiesterases in health and disease. CRC Press, Boca Raton, Florida, pp 275–301
33. Wang H, Yan Z, Geng J, Kunz S, Seebeck T, Ke H (2007) Mol Microbiol 66:1029–1038
34. Xu RX, Hassell AM, Vanderwall D, Lambert MH, Holmes WD, Luther MA, Rocque WJ, Milburn MV, Zhao Y, Ke H, Nolte RT (2000) Science 288:1822–1825
35. Read LK, Mikkelsen RB (1991) J Parasitol 77:346–352
36. Saeki T, Adachi H, Takase Y, Yoshitake S, Souda S, Saito I (1995) J Pharmacol Exp Ther 272:825–831
37. Card GL, England BP, Suzuki Y, Fong D, Powell B, Lee B, Luu C, Tabrizizad M, Gillette S, Ibrahim PN, Artis DR, Bollag G, Milburn MV, Kim SH, Schlessinger J, Zhang KY (2004) Structure 12:2237–2247
38. Verhoest PR, Chapin DS, Corman M, Fonseca K, Harms JF, Hou X, Marr ES, Menniti FS, Nelson F, O'Connor R, Pandit J, Proulx-Lafrance C, Schmidt AW, Schmidt CJ, Suiciak JA, Liras S (2009) J Med Chem 52:5188–5196